INTERNATIONAL JOURNAL OF
NUMERICAL ANALYSIS AND MODELING
Volume 14, Number 4-5, Pages 532–549

A NEW FINITE ELEMENT FOR INTERFACE PROBLEMS HAVING ROBIN TYPE JUMP

DO Y. KWAK, SEUNGWOO LEE, AND YUNKYONG HYON

Abstract. We propose a new finite element method for solving second order elliptic interface problems whose solution has a Robin type jump along the interface. We cast the problem into a new variational form and introduce a finite element method to solve it using a uniform grid. We modify the P_1-Crouzeix-Raviart element so that the shape functions satisfy the jump conditions along the interface. We note that there are cases that the Lagrange type basis can not be used because of the jump in the value. Numerical experiments are provided.

Key words. Finite element, uniform grid, interface problem, Robin type jump, P_1-Crouzeix-Raviart finite element method.

1. Introduction

In recent years, there has been an extensive research towards problems involving interface, (see [1, 15, 22, 37, 35, 39, 41] and references therein) and numerical methods for such problems. A widely studied example is an elliptic problem having discontinuous coefficients, where the solution satisfies natural jump conditions $[u] = 0$, $[\beta \frac{\partial u}{\partial n}] = 0$ across the interface immersed in domain. See [14, 21, 23, 40, 41], for example. This kind of problem typically arises from diffusion phenomena in a material consisting of heterogeneous media. Other important class of problem includes the time-dependent problems which may have a moving interface [24, 33, 38, 42], for instance, the incompressible Navier-Stokes equations for two fluids [19, 36] and an solid/solid or solid/fluid interaction problems [8, 9, 22]. In most of those examples, the primary variables, such as heat, potential, displacement and velocity, etc., or their derivatives (or flux) have certain jumps. To solve such problems numerically, for instance by finite element method, one usually need to use body fitted grids to get the optimal numerical results. But the grid generation is complicated and it is a time consuming job to solve the linear equation derived from the body fitted grids since the matrix is unstructured.

On the other hand, a new class of finite element methods have been suggested and are shown to perform quite well for interface problems, see [14, 30, 41] and references therein. These methods are called *immersed finite element methods (IFEMs)* which use non fitted (say, uniform) grid for interface problems (so the interface cuts the interior of some elements). The idea of this new method is to modify the basis functions so that they satisfy the interface conditions along the interface within each element. Although the first one of these schemes was proposed for the finite element methods using Lagrange type P_1 element having degree of freedom at vertices, the idea works well especially with Crouzeix-Raviart(CR) nonconforming basis functions [17], since the consistency error term can be shown to be optimal when CR bases are used [30].

Let us briefly review some works related to general interface conditions. Angot [46] proposed a fictitious domain method to embed a smooth domain into a

Received by the editors Dec 23, 2016 and, in revised form, April 03, 2017.
2000 *Mathematics Subject Classification.* 65N15, 65N30, 35J60.

rectangular domain and showed that the two formulations are equivalent. In the meantime, the boundary condition was transformed into an interface condition. The numerical scheme using uniform grids was proposed in [4]. They used standard piecewise linear basis function together with the local refinement to resolve the smooth interface. Similar approach using finite volume methods was earlier suggested in [3]. For the problem with natural interface conditions, Ji et al. [25] have studied similar problems using the standard basis function on each sub element, hence they need extra basis functions. Their scheme also has the problem of severe deterioration of condition number. Hence they proposed adding a ghost-penalty suggested in [12] to stabilize the condition number of the resulting matrix. There are other types of unfitted grid method, see [21], [22] and references therein, where one uses cut basis functions as extra degree of freedoms. The case of elasticity problems with homogeneous condition using rectangular grids was considered in [44] and the analysis for triangular grids is carried out in [31]. One dimensional poroelasticity problem using IIM was considered by Bean et al. [7]. Furthermore, coupled Darcy flow and Stokes flow are studied in [34] and the numerical method based on DG scheme has appeared in [47].

In this paper, we propose a new IFEM scheme using CR nonconforming basis functions which can handle jump discontinuity of different kinds. All of the schemes discussed above have certain similarity with our scheme in the sense that they all use unfitted grids. However, they are different from ours at least one of the following aspect; either (i) they treat homogenous jump condition only (the solution is thus continuous), or (ii) they use Lagrange type P_1 nodal basis functions, or (iii) they do not consider consistency terms to compensate the errors, or (iv) they use extra degrees of freedom to capture the discontinuity along the interface, or (v) their scheme have the problem of ill-conditioning for certain interface. Our scheme to be presented here does not have any disadvantages/restrictions above.

Now we describe the model equation with interface, where the jump of primary variable is related to the normal flux. These problems arise in the study of medical imaging of cancer cells such as MREIT [1, 2], problems with spring-type jumps in structural mechanics [29, 45], or electrochemotherapy [33], where the conductivity of cell membrane changes abruptly across the membrane. In the development of MREIT, for example, we encounter a partial differential equation (PDE) which models the electric behavior of biological tissue under the influence of an electric field which involves many cells. Conducting cytoplasm is surrounded by a thin insulating membrane (see Figure 1). Inside each cell Ω^i, $i = 1, \ldots, N$, the medium is homogeneous and isotropic. We assume that the conductivity of the cell Ω^i is β for all i. The outside of cells, which is denoted by Ω^0, is also composed of an isotropic homogeneous medium whose conductivity is β. Let $\Omega := \cup_{i=0}^{N} \Omega^i$ be a whole domain. The membrane of the cell is very thin and resistive. The thickness d of the membrane is very small compared to the size of the cells, i.e., $d \ll |\Omega^i|$. Since the membrane is very resistive, the conductivity of the membrane β_{mem} is close to zero. The derived model equation depends on the value of conductivity. Similar description may apply to electrochemotherapy. In such problems, the electric potential or

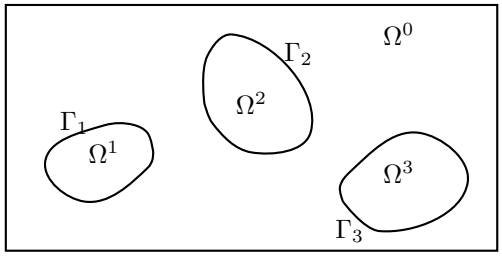

FIGURE 1. A sketch of the electric behavior of biological tissue. The regions of Ω^i,$= 1, 2, 3$ are the inside cells. The region of Ω^0 is the outside of cells.

displacement variable, etc., denoted by u is described by

$$-\nabla \cdot \beta \nabla u = f \quad \text{in } \Omega^i,\ i = 0, 1, \ldots, N, \tag{1}$$

$$[u]_{\Gamma_i} = \alpha \frac{\partial u}{\partial n}^0 \quad \text{on } \Gamma_i,\ i = 1, \ldots, N, \tag{2}$$

$$\left[\frac{\partial u}{\partial n}\right]_{\Gamma_i} = 0 \quad \text{on } \Gamma_i,\ i = 1, \ldots, N, \tag{3}$$

$$u = 0 \quad \text{on } \partial\Omega, \tag{4}$$

where the parameters α and β are bounded below and above by two positive constants and $[\cdot]_{\Gamma_i}$ denotes the jump across a C^1 simple curve Γ_i (the interface between two regions).

This kind of interface conditions is different from the case when the jumps of the solutions are given a priori (i.e., $[u] = g_1$ and $[\beta \frac{\partial u}{\partial n}] = g_2$ are given) for which some of numerical methods are proposed in [10, 13, 18, 20, 23, 35]. However, when the jump of the solution is unknown as in (2), no simple numerical methods for solving such problems are known (*even with fitted grids*). Moreover, the usual variational formulations using Sobolev theory cannot be applied directly. However, thanks to the intrinsic jump conditions (2) and (3), we can introduce a new variational formulation for these problems. For a numerical method, we design a new finite element by modifying the CR basis functions according to the jump conditions (2) and (3). Exploiting the idea from the immersed finite element [30], we can construct a new finite element. Using this element, we provide a numerical scheme based on the recent works [32, 43] where the variational forms with additional consistency and stability terms are studied. We remark that the Lagrange type shape function which takes vertex values as degree of freedom can not be used to handle this kind of jump discontinuity; when the interface passes one of the vertices, the function value at the vertex can not be specified (see Figure 3 (b)). A series of numerical experiments indicate that our method yields optimal convergence of the solution u for the model problem (1). Also, our method does not suffer from deterioration in condition number, mentioned in [26]. This seems due to the basis function having average degrees of freedom along edges, not at vertex.

The rest of the paper is organized as follows. In the next section, we describe a model equation arising from the medical imaging problems using MREIT. Then we introduce an equivalent variational formulation. In Section 3, we construct basis functions by modifying the P_1-CR nonconforming functions to satisfy the jump conditions. In Section 4, we propose a numerical scheme using the variational

formulation with the modified basis functions. Finally, in Section 5, some numerical results are presented.

2. Preliminaries

In order to derive the jump conditions (2) and (3), let us consider a biological tissue under the influence of an electric field. For simplicity, we consider the case of one cell, i.e, $N = 1$. See Figure 2, where the zoom-in part is to explain how the model equation is obtained by describing the voltage drops across the membrane. After setting up the model interface condition, the membrane is replaced by an interface of thickness zero. The electric potential of a biological tissue can be described by the following equation [1, 2, 28]

$$\begin{cases} -\nabla \cdot \beta \nabla u = f & \text{in } \Omega := \Omega^0 \cup \Omega^{mem} \cup \Omega^1, \\ u = 0 & \text{on } \partial\Omega, \end{cases} \tag{5}$$

where three sub-domains Ω^0, Ω^{mem}, and Ω^1 denote outside, membrane, and inside of the cell, respectively. The boundary of the membrane Ω^{mem} consists of two closed curves C_0 and C_1. Let $d \ll |\Omega^1|$ be the uniform thickness of the membrane region Ω^{mem}. We assume that the cytoplasm of the inside and outside cell have the same conductivity β [27, 48]. The strong resistance of the membrane implies that the conductivity of the membrane is very small compared to the conductivity of the cell, i.e. $\beta^{mem} \ll \beta$. We assume that d/β^{mem} is bounded below and above.

The natural jump conditions along the interfaces are

$$[u] = 0, \ \left[\beta \frac{\partial u}{\partial n}\right] = 0 \ \text{ across } \Gamma = C_0 \cup C_1, \tag{6}$$

where n is the unit outer normal vector. Hence along the two interfaces we have

$$\beta \frac{\partial u^1}{\partial n} = \beta^{mem} \frac{\partial u^{mem}}{\partial n} \text{ on } C_1 \text{ and } \beta^{mem} \frac{\partial u^{mem}}{\partial n} = \beta \frac{\partial u^0}{\partial n} \text{ on } C_0, \tag{7}$$

respectively. Since the membrane is very thin, we may assume that the potential u inside Ω^{mem} varies linearly along the normal direction. Hence, from (7), we obtain

$$u(b) - u(a) = \int_a^b \frac{\partial u^{mem}}{\partial n} ds \approx \int_a^b \frac{\beta}{\beta^{mem}} \frac{\partial u^0}{\partial n} ds \approx d \frac{\beta}{\beta^{mem}} \frac{\partial u^0}{\partial n}. \tag{8}$$

For small enough $0 < d \ll 1$, we assume that the curves C_0 and C_1 collapse into one interface Γ and set

$$[u] = u(b) - u(a), \quad \left[\frac{\partial u}{\partial n}\right] = \left.\frac{\partial u^1}{\partial n}\right|_{C_1} - \left.\frac{\partial u^0}{\partial n}\right|_{C_0}.$$

Thus, we obtain the jump conditions (2) and (3) with the parameter

$$\alpha = d \frac{\beta}{\beta^{mem}}, \tag{9}$$

which is related to the thickness of membrane and the ratio between the conductivities on Ω^0 and Ω^{mem}. An analysis using asymptotic expansions for such problems are given in [28].

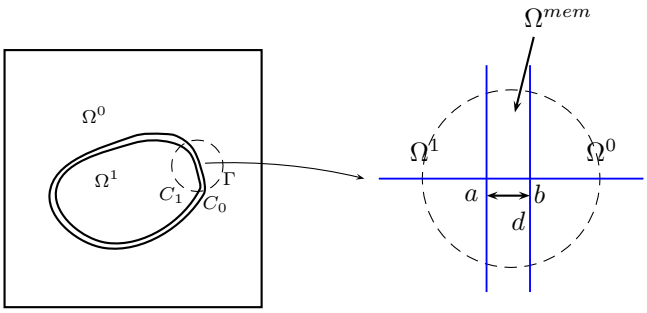

FIGURE 2. A sketch of the domain Ω and local zoom-in near membrane.

2.1. Variational form. In this subsection, we derive a variational formulation for the problem (1) - (4). For this purpose, we introduce some notations of function spaces. Let O be any domain and let $H^m(O)$, $m = 0, 1, 2$ ($H^0(O) = L^2(O)$) be a usual Sobolev space with norm $\|u\|_{m,O} = \left(\sum_{j=0}^m \int_O |\partial^j u|^2 dx\right)^{1/2}$ and we define the following spaces

$$\widetilde{H}^m(O) := H^m(\Omega^0 \cap O) \cap H^m(\Omega^1 \cap O), \tag{10}$$

$$\widetilde{H}^m_\Gamma(O) := \left\{u : u \in \widetilde{H}^m(O), [u] = \alpha \frac{\partial u^0}{\partial n}, \left[\frac{\partial u}{\partial n}\right] = 0 \text{ on } \Gamma \cap O\right\}, \tag{11}$$

$$\widetilde{H}^m_{\Gamma,0}(O) := \left\{u : u \in \widetilde{H}^m_\Gamma(O), u|_{\partial O} = 0\right\} \tag{12}$$

equipped with the (semi) norms:

$$|u|_{\widetilde{m},O} = |u|_{\widetilde{H}^m(O)} := \sum_{i=0}^1 |u|_{H^m(\Omega^i \cap O)}, \ \|u\|_{\widetilde{m},O} = \|u\|_{\widetilde{H}^m(O)} := \sum_{i=0}^1 \|u\|_{H^m(\Omega^i \cap O)}.$$

Clearly, $\widetilde{H}^m_\Gamma(\Omega)$ and $\widetilde{H}^m_{\Gamma,0}(\Omega)$ are complete subspaces of $\widetilde{H}^m(\Omega)$. We also use $\widetilde{H}^1_0(\Omega)$ to denote the space of all functions $v \in \widetilde{H}^1(\Omega)$ vanishing on $\partial\Omega$. When the domain is Ω, we write $\widetilde{H}^m$ for $\widetilde{H}^m(\Omega)$ and denote its norm by $\|u\|_{\widetilde{H}^m}$. We derive a variational form of the problem (1)–(4). Multiply (1) by any $v \in \widetilde{H}^1_0(\Omega)$ and use integration by parts on each domain to get

$$\int_{\Omega^i} \beta \nabla u \cdot \nabla v \, dx = \int_{\Omega^i} f v \, dx + \int_{\partial\Omega^i} \beta \frac{\partial u}{\partial n^i} v \, ds, \ i = 0, 1,$$

where n^i is the unit outer normal to Ω^i. Consider the line integral $\int_{\partial\Omega^i} \beta \frac{\partial u}{\partial n^i} v \, ds$, $i = 0, 1$. Since we have

$$\sum_{i=0}^1 \int_{\partial\Omega^i} \beta \frac{\partial u}{\partial n^i} v \, ds = \int_{\partial\Omega^0} \beta \frac{\partial u}{\partial n^0} v \, ds - \int_{\partial\Omega^1} \beta \frac{\partial u}{\partial n^1} v \, ds \tag{13}$$

$$= -\int_\Gamma \beta \frac{\partial u}{\partial n}[v] \, ds \tag{14}$$

$$= -\int_\Gamma \frac{\beta}{\alpha}[u][v] \, ds, \tag{15}$$

the solution $u \in \widetilde{H}^2_{\Gamma,0}(\Omega)$ of the problem (1) satisfies

$$a(u,v) := \sum_{i=0}^{1} \int_{\Omega^i} \beta \nabla u \cdot \nabla v \, dx + \int_{\Gamma} \frac{\beta}{\alpha}[u][v] \, ds = (f,v), v \in \widetilde{H}^1_0(\Omega). \tag{16}$$

Conversely, assume $u \in \widetilde{H}^2_{\Gamma,0}$ satisfy (16). Integrating by parts, we see the left hand side of (16) becomes

$$-\sum_{i=0}^{1} \int_{\Omega^i} \nabla \cdot (\beta \nabla u) v dx + \sum_{i=0}^{1} \int_{\partial\Omega^i} \beta \frac{\partial u}{\partial n^i} v \, ds + \int_{\Gamma} \frac{\beta}{\alpha}[u][v] \, ds. \tag{17}$$

Let v vanish on Γ. Then we have the following equation.

$$-\sum_{i=0}^{1} \int_{\Omega^i} \nabla \cdot (\beta \nabla u) v dx = \int_{\Omega} f v \, dx, \forall v \in \widetilde{H}^1_0(\Omega) \cap \{v|_{\Gamma} = 0\}.$$

Hence it holds that

$$-\nabla \cdot (\beta \nabla u) = f \text{ in } \Omega^0 \cup \Omega^1.$$

From (16), (17), we have

$$0 = -\int_{\partial\Omega^0} \beta \frac{\partial u}{\partial n^0} v \, ds + \int_{\partial\Omega^1} \beta \frac{\partial u}{\partial n^1} v \, ds + \int_{\Gamma} \frac{\beta}{\alpha}[u][v] \, ds, \tag{18}$$

for all $v \in \widetilde{H}^1_0(\Omega)$. Choosing v with $[v] = 0$ on Γ, we see

$$\left[\frac{\partial u}{\partial n}\right] = 0 \text{ on } \Gamma$$

and hence, from (18), we obtain the condition (2) by setting $v|_{\Omega^1} = 0$.

3. A new finite element based on P_1-Crouzeix-Raviart element

In this section, we propose a finite element for solving the variational form (16). For this purpose, we need to construct an approximate subspace of $\widetilde{H}^1_{\Gamma,0}(\Omega)$. At first glance, a natural approach is to triangularize the domain aligning the grids with the interface and then discretize the space by piecewise linear functions incorporating the jump conditions along the interface. However, basis functions have to be designed to satisfy the jump conditions (2) and (3) along the edge (which is aligned with the interface) of an element. Such process may be a nontrivial matter unless a discontinuous Galerkin method is used. Instead, we propose a new approach with a non-fitted grid, similar to the IFEM, which allows the interface cut through the element. In this way, the basis functions are completely determined by the degrees of freedom and the jump conditions on each element.

Although our method can be applied to any reasonable domains, we take a rectangle domain for simplicity. We assume a quasi-uniform triangulation $\{\mathcal{T}_h\}$ of Ω by triangles of maximum size h is given [16]. In general, the mesh does not align the smooth interface. We call an element $T \in \mathcal{T}_h$ an *interface element* if the interface Γ passes through the interior of T, otherwise we call T a *non-interface element*.

For a non-interface element $T \in \mathcal{T}_h$, we simply use the standard P_1-Crouzeix-Raviart nonconforming functions [17] on T having the averages along each edge as degrees of freedom, and use $N_h(T)$ to denote the linear spaces spanned by the three basis functions on T: Let e_i, $i = 1, 2, 3$ be the edges of T. Then

$$N_h(T) = \text{span}\left\{\phi_i : \phi_i \text{ is linear on } T \text{ and } \overline{\phi_i}\big|_{e_j} := \frac{1}{|e_j|}\int_{e_j} \phi_i ds = \delta_{ij}, i, j = 1, 2, 3\right\}.$$

We now construct local basis functions on an interface element, using the jump conditions given above. Consider a typical reference interface element T having vertices at $A_1(0,0)$, $A_2(1,0)$ and $A_3(0,1)$ (see Figure 3 (a)). We assume that the interface meets with the edges at $D(x_0,0)$ and $E(0,y_0)$ $(0 < x_0, y_0 \leq 1)$ and we replace the curved interface by the line segment $\overline{DE}$. The unit normal vector to the line segment is $\mathbf{n}_{\overline{DE}} = (y_0, x_0)/\sqrt{x_0^2 + y_0^2}$.

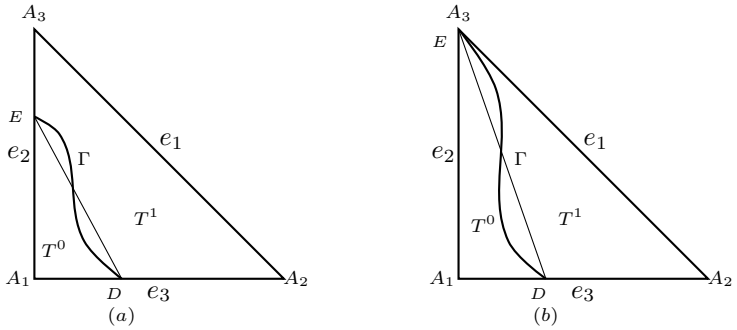

FIGURE 3. A typical reference interface triangle.

For any given values v_i, $(i = 1, 2, 3)$, we can construct a piecewise linear function ϕ (see [30]) of the form

$$\phi(x,y) = \begin{cases} \phi^0(x,y) = a_0 + b_0 x + c_0 y, & (x,y) \in T^0, \\ \phi^1(x,y) = a_1 + b_1 x + c_1 y, & (x,y) \in T^1 \end{cases} \tag{19}$$

satisfying

$$\frac{1}{|e_i|}\int_{e_i} \phi \, ds = v_i, \ i = 1,2,3, \tag{20}$$

$$\phi^0 - \phi^1 = \alpha \frac{\partial \phi^0}{\partial \mathbf{n}_{\overline{DE}}} \text{ at } D \text{ and } E, \tag{21}$$

$$\frac{\partial \phi^0}{\partial \mathbf{n}_{\overline{DE}}} = \frac{\partial \phi^1}{\partial \mathbf{n}_{\overline{DE}}} \text{ along } \overline{DE}. \tag{22}$$

If we choose $(v_1, v_2.v_3) = (1,0,0), = (0,1,0)$ or $(0,0,1)$ we obtain three local basis functions.

Proposition 3.1. *There exists a unique piecewise linear function of the form (19) satisfying (20)-(22).*

Proof. The condition (20) gives the following three equations:

$$\bar{\phi}|_{e_1} = a_0 + \frac{1}{2}b_0 + \frac{1}{2}c_0 = v_1 \tag{23}$$

and

$$\begin{aligned} \bar{\phi}|_{e_2} &= \int_{e_2} \phi \, ds = \int_{\overline{A_1E}} \phi^1 \, ds + \int_{\overline{EA_3}} \phi^0 \, ds \\ &= (a_1 + \frac{y_0}{2}c_1)y_0 + (a_0 + \frac{y_0+1}{2}c_0)(1-y_0) = v_2, \end{aligned} \tag{24}$$

where we used mid-point quadrature on $\overline{A_1E}$ and $\overline{EA_3}$. Similarly, we have

$$\bar{\phi}|_{e_3} = (a_1 + \frac{x_0}{2}b_1)x_0 + (a_0 + \frac{x_0+1}{2}b_0)(1-x_0) = v_3. \tag{25}$$

From the jump condition (21), we have

$$a_0 + b_0x_0 = a_1 + b_1x_0 + \alpha(b_0n_1 + c_0n_2), \tag{26}$$

$$a_0 + c_0y_0 = a_1 + c_1y_0 + \alpha(b_0n_1 + c_0n_2), \tag{27}$$

where n_1 and n_2 are the components of $\mathbf{n}_{\overline{DE}}$. The last condition (22) is

$$(b_0n_1 + c_0n_2) = (b_1n_1 + c_1n_2). \tag{28}$$

Then the coefficient matrix of the above linear system for the unknowns a_0, b_0, c_0 and a_1, b_1, c_1 in this order is

$$\mathcal{A} = \begin{pmatrix} 1 & \frac{1}{2} & \frac{1}{2} & 0 & 0 & 0 \\ 1-y_0 & 0 & \frac{1}{2}(1-y_0^2) & y_0 & 0 & \frac{1}{2}y_0^2 \\ 1-x_0 & \frac{1}{2}(1-x_0^2) & 0 & x_0 & \frac{1}{2}x_0^2 & 0 \\ 1 & x_0-\alpha n_1 & -\alpha n_2 & -1 & -x_0 & 0 \\ 1 & -\alpha n_1 & y_0-\alpha n_2 & -1 & 0 & -y_0 \\ 0 & n_1 & n_2 & 0 & -n_1 & -n_2 \end{pmatrix}. \tag{29}$$

Adding last three columns to the first three, and obvious row operations gives

$$\begin{pmatrix} 1 & \frac{1}{2} & \frac{1}{2} & 0 & 0 & 0 \\ 1 & 0 & \frac{1}{2} & y_0 & 0 & \frac{1}{2}y_0^2 \\ 1 & \frac{1}{2} & 0 & x_0 & \frac{1}{2}x_0^2 & 0 \\ 0 & -\alpha n_1 & -\alpha n_2 & -1 & -x_0 & 0 \\ 0 & -\alpha n_1 & -\alpha n_2 & -1 & 0 & -y_0 \\ 0 & 0 & 0 & 0 & -n_1 & -n_2 \end{pmatrix} \sim \begin{pmatrix} 1 & \frac{1}{2} & \frac{1}{2} & 0 & 0 & 0 \\ 0 & -\frac{1}{2} & 0 & y_0 & 0 & \frac{1}{2}y_0^2 \\ 0 & 0 & -\frac{1}{2} & x_0 & \frac{1}{2}x_0^2 & 0 \\ 0 & -\alpha n_1 & -\alpha n_2 & -1 & -x_0 & 0 \\ 0 & 0 & 0 & 0 & x_0 & -y_0 \\ 0 & 0 & 0 & 0 & -n_1 & -n_2 \end{pmatrix}. \tag{30}$$

We can easily see that

$$\det(\mathcal{A}) = (-x_0n_2 - y_0n_1)\det\begin{pmatrix} -\frac{1}{2} & 0 & y_0 \\ 0 & -\frac{1}{2} & x_0 \\ -\alpha n_1 & -\alpha n_2 & -1 \end{pmatrix} \tag{31}$$

$$= (-x_0n_2 - y_0n_1)(-\frac{1}{2}(\frac{1}{2} + \alpha n_2x_0) - \alpha n_1(\frac{1}{2}y_0)) \tag{32}$$

$$= \frac{\sqrt{x_0^2+y_0^2}}{2}(\frac{1}{2} + \alpha\sqrt{x_0^2+y_0^2}) > 0 \tag{33}$$

for any $(x_0, y_0) \neq (0, 0)$. Hence, the basis function exists uniquely on the interface element. □

For a general element T, let $\widehat{N}_h(T)$ be the linear space consisting of the shape functions constructed by their counterparts on the reference element through the standard affine mapping. Figure 4 shows graphs of typical local (discontinuous) shape functions constructed this way. We define the *finite element space* $\widehat{N}_h(\Omega)$ as the collection of functions $\hat{\phi}$ such that

$$\begin{cases} \hat{\phi}|_T \in N_h(T), \text{ if } T \text{ is a noninterface element;} \\ \hat{\phi}|_T \in \widehat{N}_h(T), \text{ if } T \text{ is an interface element;} \\ \text{if } T_1 \text{ and } T_2 \text{ share an edge } e, \text{ then} \\ \displaystyle\int_e \hat{\phi}|_{\partial T_1} ds = \int_e \hat{\phi}|_{\partial T_2} ds; \text{ and } \int_{\partial T \cap \partial\Omega} \hat{\phi}\, ds = 0. \end{cases}$$

Lastly, we let $H_h(\Omega) := \widetilde{H}^1_{\Gamma,0}(\Omega) + \widehat{N}_h(\Omega)$.

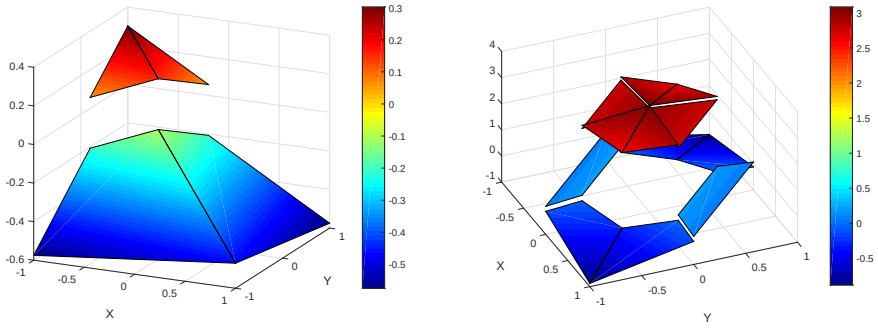

FIGURE 4. Some shape of functions in $\widehat{N}_h(\Omega)$ - left figure shows a function $\hat{\phi}$ on two interface elements and the right shows a function $\hat{\phi}$ on six interface elements.

Next, we define the interpolation operator. For any $u \in \widetilde{H}^1_\Gamma(T)$, we let $\hat{I}_h u$ be the the finite element function in $\widehat{N}_h(T)$ satisfying

$$\int_{e_i} \hat{I}_h u \, ds = \int_{e_i} u \, ds; \ i = 1, 2, 3,$$

where e_i, $i = 1, 2, 3$ are the edges of T. We call $\hat{I}_h u$ the local *interpolant* of u in $\widehat{N}_h(T)$ and we naturally extend it to $\widetilde{H}^1_\Gamma(\Omega)$ by $(\hat{I}_h u)|_T = \hat{I}_h(u|_T)$ for each T.

4. Numerical scheme

In this section, we propose a numerical scheme using the finite element space in Section 3. First, we consider a natural discrete variational formulation of (16): find the discrete solution $u_h \in \widehat{N}_h(\Omega)$ such that

$$a_h(u_h, v_h) = (f, v_h), \quad \forall v_h \in \widehat{N}_h(\Omega), \tag{34}$$

where

$$a_h(u_h, v_h) := \sum_{T \in \mathcal{T}_h} \sum_{i=0}^{1} \int_{T \cap \Omega^i} \beta \nabla u_h \cdot \nabla v_h \, dx + \int_\Gamma \frac{\beta}{\alpha} [u_h][v_h] \, ds, \tag{35}$$

for $u_h, v_h \in H_h(\Omega)$. Since we use the modified CR element, the error in the consistency term of (34) is not optimal. From the numerical results in Section 5, we can see that this scheme does not provide optimal convergence.

To remedy the inconsistency occurred along the boundary of interface elements, we insert consistency and stability terms to the discrete variational formulation. Such ideas are used in many numerical methods, for example, discontinuous Galerkin methods [6, 5, 11] and IFEMs [32, 43]. For this purpose, we proceed as follows. The collection of all interior edges of triangulation $\mathcal{T}_h$ is denoted by $\mathcal{E}_h$. To determine the signed jump, we associate a normal n_e for each edge e once and for all. Let $e \in \mathcal{E}_h$ be an interior edge shared by elements T_1 and T_2. We define the jump $[\phi]$ and average $\{\phi\}$ of function $\phi \in H_h(T_1 \cup T_2)$ on the edge e by

$$[\phi] = \phi_1 - \phi_2, \quad \{\phi\} = \frac{1}{2}(\phi_1 + \phi_2),$$

where $\phi_i = \phi|_{T_i}$, $i = 1, 2$. Multiplying $v \in \widehat{N}_h(\Omega)$ to equation (1) and applying Green's theorem, we have

$$\sum_{T\in\mathcal{T}_h}\sum_{i=0}^{1}\int_{T\cap\Omega^i}\beta\nabla u\cdot\nabla v\,dx-\int_{\partial\Omega^i\cap T}\beta\frac{\partial u}{\partial n^i}v\,ds$$

$$-\sum_{e\in\mathcal{E}_h}\int_e\left\{\beta\frac{\partial u}{\partial n}\right\}[v]\,ds=\sum_{T\in\mathcal{T}_h}\int_T fv\,dx. \tag{36}$$

By (13) - (15) and the fact that $[u] = 0$ for every edge $e \in \mathcal{E}_h$, the equation (36) is equivalent to the following equation,

$$\sum_{T\in\mathcal{T}_h}\sum_{i=0}^{1}\int_{T\cap\Omega^i}\beta\nabla u\cdot\nabla v\,dx+\int_{\Gamma\cap T}\frac{\beta}{\alpha}[u][v]\,ds \tag{37}$$

$$-\sum_{e\in\mathcal{E}_h}\int_e\left\{\beta\frac{\partial u}{\partial n}\right\}[v]+\left\{\beta\frac{\partial v}{\partial n}\right\}[u]\,ds+\sum_{e\in\mathcal{E}_h}\int_e\frac{\sigma}{h}[u][v]\,ds=\sum_{T\in\mathcal{T}_h}\int_T fv\,dx, \tag{38}$$

where $\sigma > 0$ is some parameter. Now we define the following bilinear form : for any $u_h, v_h \in \widehat{N}_h(\Omega)$,

$$\widetilde{a}_h(u_h, v_h) := a_h(u_h, v_h) + J_1(u_h, v_h) + J_2(u_h, v_h), \tag{39}$$

where

$$J_1(u_h, v_h) = -\sum_{e\in\mathcal{E}_h}\int_e\left\{\beta\frac{\partial u_h}{\partial n}\right\}[v_h]+\left\{\beta\frac{\partial v_h}{\partial n}\right\}[u_h]\,ds, \tag{40}$$

$$J_2(u_h, v_h) = \sum_{e\in\mathcal{E}_h}\int_e\frac{\sigma}{h}[u_h][v_h]\,ds. \tag{41}$$

We are now ready to define our *finite element method*: find $u_h \in \widehat{N}_h(\Omega)$ such that

$$\widetilde{a}_h(u_h, \phi_h) \quad = \quad (f, \phi_h),\ \forall\phi_h \in \widehat{N}_h(\Omega). \tag{42}$$

Note that this is a consistent scheme in the sense that for the exact solution u, we have

$$\widetilde{a}_h(u, \phi_h) \quad = \quad (f, \phi_h),\ \forall\phi_h \in \widehat{N}_h(\Omega). \tag{43}$$

4.1. Error estimate. Instead of proving a complete error estimate, we only sketch the framework using the Lax - Milgram theorem, since most of the techniques are well known, but the interpolation error estimate seems different from the standard case. First introduce the mesh dependent norm $|\!|\!| \cdot |\!|\!|$ on the space $H_h(\Omega)$,

$$|\!|\!|v|\!|\!|^2 \quad := \quad \sum_{T\in\mathcal{T}_h}\left\|\sqrt{\beta}\nabla v\right\|^2_{0,T}+\sum_{e\in\mathcal{E}_h}h^{-1}\left\|[\sqrt{\beta}v]\right\|^2_{0,e}.$$

Clearly, $\widetilde{a}_h(\cdot,\cdot)$ is bounded on $\widehat{N}_h(\Omega)$ with respect to $|\!|\!| \cdot |\!|\!|$:

$$|\widetilde{a}_h(u, v)| \le C_b|\!|\!|u|\!|\!||\!|\!|v|\!|\!|,\ \forall u, v \in \widehat{N}_h(\Omega). \tag{44}$$

Next, we can prove the coerciveness of the form $\widetilde{a}_h(\cdot,\cdot)$ in a similar fashion to [32], [43].

Lemma 4.1. *There exists a positive constant C_c independent of v_h such that for all $v_h \in \widehat{N}_h(\Omega)$ the following holds:*

$$\widetilde{a}_h(v_h, v_h) \ge C_c|\!|\!|v_h|\!|\!|^2. \tag{45}$$

Then the error estimate reduces to the estimate of interpolation error:

TABLE 1. Numerical results for the cases of elliptical interface with the consistent scheme in Example 5.1.

$1/h$	$\|u-u_h\|_{0,\Omega}$	*Order*	$\|u-u_h\|_{1,h}$	*Order*
8	*3.359148E-2*		*8.778087E-1*	
16	*7.480368E-3*	*2.167*	*4.307915E-1*	*1.027*
32	*1.820215E-3*	*2.039*	*2.142997E-1*	*1.007*
64	*4.666885E-4*	*1.964*	*1.071044E-1*	*1.001*
128	*1.161599E-4*	*2.006*	*5.343991E-2*	*1.003*
256	*2.888874E-5*	*2.008*	*2.669799E-2*	*1.001*
512	*7.207460E-6*	*2.003*	*1.334396E-2*	*1.001*

Theorem 4.1. *Let u (resp. u_h) be the solution of (16) (resp. (43). Then there exists a positive constant C independent of u and h such that*

$$\|\!|u-u_h|\!\| \quad \leq \quad C\|\!|u-\hat{I}_h u|\!\|.$$

Proof. By Lemma 4.1, (43), (44) and (45) we get the result. □

Remark 4.1. *The difficulty of estimating the interpolation error lies in the inapplicability of the Bramble - Hilbert type Lemma. It is due to the fact that functions are discontinuous, unlike as earlier case* [30]. *Since the numerical experiments in Section 5 suggest optimal order of convergence, we leave this topic as a future work.*

5. Numerical experiments

We solve the model problem (1)-(3) on the domain $\Omega = [-1,1]\times[-1,1]$ which is partitioned into uniform right triangles having the base size $h = 2^{-k}$. For all the numerical tests, we take $\beta = 1$ except Example 5.4 where discontinuous coefficients $\beta^- = 1$, and $\beta^+ = 5$ are used. We consider various interfaces described by the zero level set of some analytic functions. The discrete system is solved by conjugate gradient method preconditioned by diagonals. The CPU time (the worst case) is reported for Example 5.5.

Example 5.1. *We consider an elliptical interface*

$$\Gamma = \left\{(x,y) : \frac{x^2}{a^2}+\frac{y^2}{b^2} = r_0^2\right\},$$

where $a = 0.7$, $b = 0.3$, and $r_0 = 1$. In this example, we set

$$\alpha = \alpha_0 r_0 / \sqrt{\frac{x^2}{a^4}+\frac{y^2}{b^4}},$$

where $\alpha_0 = 50$.

The exact solution is

$$u = \begin{cases} u^- = \dfrac{1}{2}\left(\dfrac{x^2}{a^2}+\dfrac{y^2}{b^2}\right) - \alpha_0 r_0, & \text{for } \frac{x^2}{a^2}+\frac{y^2}{b^2} < r_0^2, \\ u^+ = \dfrac{1}{2}\left(\dfrac{x^2}{a^2}+\dfrac{y^2}{b^2}\right), & \text{for } \frac{x^2}{a^2}+\frac{y^2}{b^2} > r_0^2. \end{cases} \tag{46}$$

The numerical results by the consistent method are presented in Table 1 and the numerical solution is plotted in Figure 5. We observe optimal L^2- and H^1-errors.

For comparison, we also test the inconsistent scheme (34). Table 2 shows the numerical results of the inconsistent scheme. Although the convergence rate in H^1-error maintains the optimal convergence, we see the deterioration of convergence

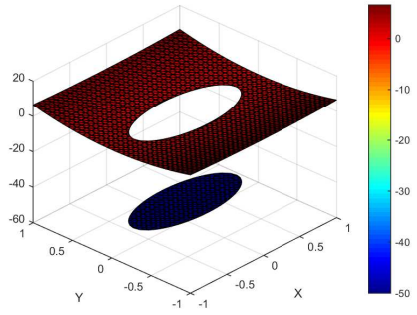

FIGURE 5. Plots of numerical solution in Example 1 computed by the consistent scheme.

rate in L^2-error when the mesh becomes finer. Figure 6 shows the plot of the solution. We observe that the error of the inconsistent method is much larger than that of the consistent method. We see that the consistency terms (41) in the bilinear form play an important role in obtaining stable solutions.

TABLE 2. Numerical results for the cases of elliptical interface with the inconsistent scheme in Example 5.1

$1/h$	$\|u-u_h\|_{0,\Omega}$	*Order*	$\|u-u_h\|_{1,h}$	*Order*
8	*2.743981E-1*		*1.084094E-0*	
16	*1.365865E-1*	*1.006*	*5.177826E-1*	*1.066*
32	*3.467153E-2*	*1.978*	*2.487899E-1*	*1.057*
64	*7.393499E-3*	*2.229*	*1.171032E-1*	*1.087*
128	*2.806019E-3*	*1.398*	*5.808841E-2*	*1.011*
256	*9.928719E-4*	*1.499*	*2.838702E-2*	*1.033*
512	*3.063885E-4*	*1.696*	*1.398787E-2*	*1.021*

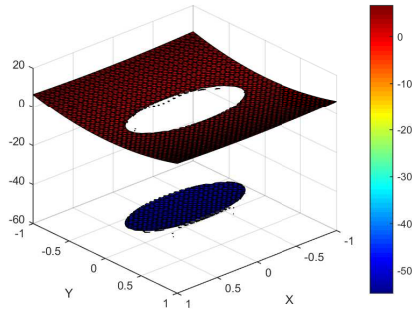

FIGURE 6. Plots of numerical solution in Example 1 by inconsistent scheme.

Example 5.2. *In this example, there are four circular interfaces:*

$$\Gamma_1 = \{(x,y) : (x-0.5)^2 + (y-0.5)^2 - r_1^2 = 0\},$$
$$\Gamma_2 = \{(x,y) : (x+0.5)^2 + (y-0.5)^2 - r_2^2 = 0\},$$
$$\Gamma_3 = \{(x,y) : (x+0.5)^2 + (y+0.5)^2 - r_3^2 = 0\},$$
$$\Gamma_4 = \{(x,y) : (x-0.5)^2 + (y+0.5)^2 - r_4^2 = 0\},$$

where $(r_1, r_2, r_3, r_4) = (0.2, 0.4, 0.2, 0.3)$. *We denote the level-set of* $L_i(x,y)$ *to be interface* Γ_i. *The parameter* α *is chosen as*

$$\alpha = \begin{cases} \alpha_1 = \dfrac{10}{L_2(x,y)L_3(x,y)L_4(x,y)} & \text{on } \Gamma_1, \\ \alpha_2 = \dfrac{10}{L_1(x,y)L_3(x,y)L_4(x,y)} & \text{on } \Gamma_2, \\ \alpha_3 = \dfrac{10}{L_1(x,y)L_2(x,y)L_4(x,y)} & \text{on } \Gamma_3, \\ \alpha_4 = \dfrac{10}{L_1(x,y)L_2(x,y)L_3(x,y)} & \text{on } \Gamma_4. \end{cases} \tag{47}$$

The exact solution u *is*

$$u = \begin{cases} u_1^- = L(x,y) - 20r_1 & \text{if } L_1(x,y) < 0, \\ u_2^- = L(x,y) - 20r_2 & \text{if } L_2(x,y) < 0, \\ u_3^- = L(x,y) - 20r_3 & \text{if } L_3(x,y) < 0, \\ u_4^- = L(x,y) - 20r_4 & \text{if } L_4(x,y) < 0, \\ u^+ = L(x,y) & \text{otherwise}, \end{cases} \tag{48}$$

where $L(x,y) = L_1(x,y)L_2(x,y)L_3(x,y)L_4(x,y)$. *We observe optimal* L^2- *and* H^1-*errors from Table 3. Figure 7 shows the plot of the numerical solution.*

TABLE 3. Multiple circular interfaces in Example 5.2.

$1/h$	$\|u-u_h\|_{0,\Omega}$	*Order*	$\|u-u_h\|_{1,h}$	*Order*
8	*2.175371E-1*		*4.320518E-0*	
16	*3.760577E-2*	*2.532*	*1.999565E-0*	*1.112*
32	*8.702026E-3*	*2.112*	*9.857387E-1*	*1.020*
64	*1.936434E-3*	*2.168*	*4.892841E-1*	*1.011*
128	*4.604108E-4*	*2.072*	*2.434814E-1*	*1.007*
256	*1.081562E-4*	*2.090*	*1.214450E-1*	*1.004*
512	*2.733338E-5*	*1.984*	*6.065095E-2*	*1.002*

Example 5.3. *Here, we carry out a numerical experiment for some problem arising from spectroscopic imaging* [1]. *We consider the case of nine circular cells in the medium and assume that the properties of each cell are identical. Let the ratio between the membrane thickness and the size of the cell be* $d = 0.7 \times 10^{-3}$. *The conductivity of the medium and the cell is* $\beta = 0.5 Sm^{-1}$ *and the conductivity of the membrane is* $\beta_{mem} = 10^{-8} Sm^{-1}$. *Then by definition of the parameter* α *in (9), we have* $\alpha = 35000$. *We set the boundary value given by the function* $\sin(xy)$. *Note that there is no known analytical solution for this example. The numerical solution is depicted in Figure 8. We observe that our numerical scheme can capture the jump of the solution clearly for the problem with realistic parameters.*

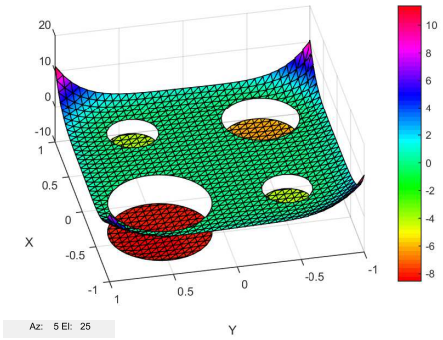

FIGURE 7. Numerical solution in Example 5.2.

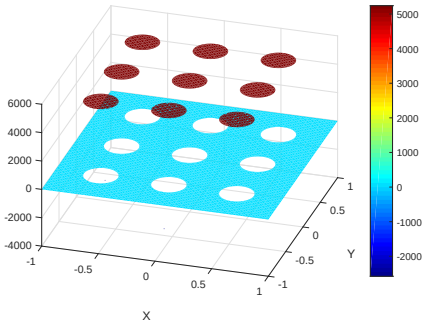

FIGURE 8. Numerical solution in Example 5.3.

Example 5.4 (Discontinuous coefficients)**.** *We run Example 1 with* $\beta^- = 1$ *and* $\beta^- + = 5$. *We again see optimal result. See Table 3 and left of Figure 9.*

TABLE 4. Distinct β case, $\beta^- = 1$, $\beta^+ = 5$.

$1/h$	$\|u - u_h\|_{0,\Omega}$	*Order*	$\|u - u_h\|_{1,h}$	*Order*
8	*5.289152E-3*		*6.437354E-2*	
16	*1.107621E-3*	*2.256*	*3.068055E-2*	*1.069*
32	*2.802846E-4*	*1.983*	*1.546753E-2*	*0.988*
64	*6.844158E-5*	*2.034*	*7.558473E-3*	*1.033*
128	*1.685942E-5*	*2.021*	*3.734281E-3*	*1.017*
256	*3.532443E-6*	*2.255*	*1.841684E-3*	*1.020*
512	*8.766970E-7*	*2.011*	*9.173182E-4*	*1.006*

Example 5.5 (Non convex interface)**.** *Finally, we consider a non convex interface (with variable coefficients):*

$$\Gamma = \left\{ (x, y) : \frac{x^4}{2} - \frac{x^2}{4} + y^2 = r_0^2 \right\}.$$

TABLE 5. Peanut-shaped(Non convex) interface in Example 5.5.

$1/h$	$\|u-u_h\|_{0,\Omega}$	*Order*	$\|u-u_h\|_{1,h}$	*Order*
8	*1.821174E-2*		*2.362401E-1*	
16	*3.745501E-3*	*2.282*	*1.113194E-1*	*1.086*
32	*7.594901E-4*	*2.302*	*5.391461E-2*	*1.046*
64	*1.751442E-4*	*2.116*	*2.674545E-2*	*1.011*
128	*4.111807E-5*	*2.091*	*1.329229E-2*	*1.009*
256	*9.989118E-6*	*2.041*	*6.631906E-3*	*1.003*
512	*2.452835E-7*	*2.026*	*3.311642E-3*	*1.002*

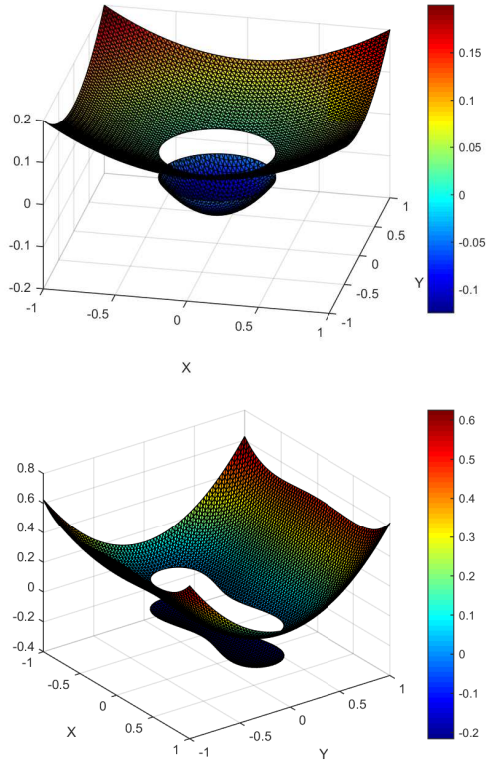

FIGURE 9. Figures for Examples 5.4 and 5.5.

The exact solution u and α are given by, with $r_0 = 0.037$,

$$\alpha = 0.2\left(\left(x^3 - \frac{x}{4}\right)^2 + y^2\right)^{-1/2}, \tag{49}$$

$$u = \begin{cases} u^- = \dfrac{1}{2}\left(\dfrac{x^4}{2} - \dfrac{x^2}{4} + y^2\right) - 1, & \text{when } \frac{x^4}{2} - \frac{x^2}{4} + y^2 < r_0^2, \\ u^+ = \dfrac{1}{2}\left(\dfrac{x^4}{2} - \dfrac{x^2}{4} + y^2\right), & \text{when } \frac{x^4}{2} - \frac{x^2}{4} + y^2 > r_0^2. \end{cases} \tag{50}$$

Table 5 and the right of Figure 9 presents the corresponding numerical solution. As a reference, we report the CPU time for the case of 512×512 grids was about

26 min. on a window based PC with Intel processor i5-4670, 3.4 Giga Hz. For all other problems, the CPU time was similar.

6. Conclusion and discussion

In this work, we proposed a new numerical method to solve interface problems where the jump of primary variable is related to the normal flux. We use CR type immersed finite element [30] to construct a new finite element which satisfies the interface conditions (2) and (3). Our numerical scheme contains consistency and stability terms to compensate the inconsistency along the boundary of the interface elements. We observe that our scheme yields optimal convergence of the solution for a variety of numerical results. The (interpolation) error analysis of this scheme is left for a future work.

Acknowledgments

The first author is supported by NRF, No. 2014R1A2A1A11053889 and the third author is supported by NIMS, No. A21100000.

References

[1] H. Ammari, J. Garnier, L. Giovangigli, W. Jing, and J. K. Seo, Spectroscopic imaging of a dilute cell suspension, J. Math. Pures Appl. 105 (2016) pp. 603–661.
[2] H. Ammari, J. Garnier, H. Kang, M. Lim, and S. Yu, Generalized Polarization Tensors for Shape Description, Numer. Math. 126 (2014) pp. 199–224.
[3] Ph. Angot, Finite volume methods for non smooth solution of diffusion models; application to imperfect contact problems in: O.P. Iliev, M.S. Kaschiev, S.D. Margenov, Bl.H. Sendov, P.S. Vassilevski (Eds.), Recent Advances in Numerical Methods and Applications. Proc. 4th Int. Conf. NMA98, Sofia (Bulgarie), World Sci. Pub., (1999) pp. 621–629.
[4] Ph. Angot, A unified fictitious domain model for general embedded boundary conditions, C. R. Acad. Sci. Paris, Serie I Math. 341 (2005), no. 11, pp. 683–688.
[5] D. N. Arnold, An interior penalty finite element method with discontinuous elements, SIAM J. Numer. Anal. 19 (1982) pp. 742–760.
[6] D. N. Arnold, F. Brezzi, B. Cockburn, and L. D. Marini, Unified analysis of discontinuous Galerkin methods for elliptic problems, SIAM J. Numer. Anal. 39 (2001) pp. 1749–1779.
[7] M. Bean and Son-Young Yi, An immersed interface method for a 1D poroelasticity problem with discontinuous coefficients, J. Comp. App. Math., V 272, (2014), pp. 81–96.
[8] R. Becker, E. Burman, and P. Hansbo, A Nitsche extended finite element method for incompressible elasticity with discontinuous modulus of elasticity, Comp. Methods Appl. Mech. Engrg. 198 (2009) pp. 3352–3360.
[9] A. Bermudez, R. Duran, and R. Rodriguez, Finite element solution of incompressible Fluid Structure vibration problems, Internat. J. Numer. Methods Engrg. 40 (1997) pp. 1435–1448.
[10] P. A. Berthelsen, A decomposed immersed interface method for variable coefficient elliptic equations with non-smooth and discontinuous solutions, J. Comp. Phys. 197 (2004) pp. 364–386.
[11] F. Brezzi, G. Manzini, D. Marini, P. Pietra, and A. Russo, Discontinuous Galerkin approximations for elliptic problems, Numer. Meth. P.D.E. 16 (2000) pp. 365–378.
[12] E. Burman, Ghost penalty, C. R. Math Acad Sci Paris 348 (2010), pp. 1217–1220.
[13] K. S. Chang and Do Y. Kwak, Discontinuous Bubble scheme for elliptic problems with jumps in the solution, Comp. Meth. Appl. Mech. Engrg. 200 (2011) pp. 494–508.
[14] S. H. Chou, D. Y. Kwak, and K. T. Wee, Optimal convergence analysis of an immersed interface finite element method, Adv. Comp. Math, 33 (2010) pp. 149–168.
[15] Z. Chen and J. Zou, Finite element methods and their convergence for elliptic and parabolic interface problems, Numer. Math. 79 (1998) pp. 175–202.
[16] P. G. Ciarlet, The finite element method for elliptic problems, North Holland 1978.
[17] M. Crouzeix and P. A. Raviart, Conforming and nonconforming finite element methods for solving the stationary Stokes equations, RAIRO Anal. Numér. 7 (1973) pp. 33–75.
[18] Y. Gong, B. Li, and Z. Li, Immersed-interface finite-element methods for elliptic interface problems with nonhomogeneous jump conditions, SIAM J. Numer. Anal. 46 (2008) pp. 472–495.

[19] S. Groβ, V. Reichelt, and A. Reusken, A finite element based level set method for two-phase incompressible flows, Comp. Visual Sci. 9 (2006) pp. 239–257.
[20] G. Guyomarc'h, C. O. Lee, and K. Jeon, A discontinuous Galerkin method for elliptic interface problems with application to electroporation, Commun. Numer. Meth. Engng 25 (2009) pp. 991–1008.
[21] A. Hansbo and P. Hansbo, An unfitted finite element method, based on Nitsche's method, for elliptic interface problems, Comp. Methods Appl. Mech. Engrg. 191 (2002) pp. 5537–5552.
[22] A. Hansbo and P. Hansbo, A finite element method for the simulation of strong and weak discontinuities in solid mechanics, Comp. Methods Appl. Mech. Engrg. 193 (2004) pp. 3523–3540.
[23] X. He, T. Lin, and Y. Lin, Immersed finite element methods for elliptic interface problems with non-homogeneous jump conditions, Int. J. Numer. Anal. Model. 8 (2011) pp. 284–301.
[24] X. He, T. Lin, Y. Lin, and X. Zhang, Immersed finite element methods for parabolic equations with moving interface, Numer. Methods P.D.E, 29 (2013) pp. 619–646.
[25] Ji, H. F., Chen, J. R., & Li, Z. L., A symmetric and consistent immersed finite element method for interface problems, J. of Sci. Comp., 61 (2014) pp. 533-557.
[26] H. Ji, J.u Chen, F. Wang, Unfitted finite element methods for the heat conduction in composite media with contact resistance, Numer. Meth. P.D.Es, 33(1) (2017) pp. 354-380.
[27] J. Keener and J. Sneyd, Mathematical Physiology, Springer New York 2009.
[28] A. Khelifia and H. Zribib, Asymptotic expansions for the voltage potentials with two-dimensional and three-dimensional thin interfaces, Math. Meth. Appl. Sci. 34 (2011) pp. 2274–2290.
[29] S. Kim, J. K. Seo, and T. Ha, A Nondestructive Evaluation Method for Concrete Voids: Frequency Differential Electrical Impedance Scanning, SIAM J. Appl. Math. 69 (2009) pp. 1759–1771.
[30] D. Y. Kwak, K. T. Wee, and K. S. Chang, An analysis of a broken P_1-nonconforming finite element method for interface problems, SIAM J. Numer. Aanal. 48 (2012) pp. 2117–2134.
[31] D. Y. Kwak, S. Jin, and D. Kyeong , A stabilized P_1-immersed finite element method for the interface for elasticity problems, ESAIM: M^2AN, V. 51 (2017) pp. 187–207.
[32] D. Y. Kwak and J. Lee, A modified P_1-immersed finite element method, Int. J. Pure Appl. Math. 104 (2015) pp. 471–494.
[33] I. Lackovic, R. Magjarevic, and D. Miklavcic, Analysis of Tissue Heating During Electroporation Based Therapy: A 3D FEM Model for a Pair of Needle Electrodes, Medicon 2007 IFMBE Proceedings 16, (2007) pp. 631–634.
[34] W. J. Layton, F. Schieweck, and I. Yotov, Coupling fluid flow with porous media flow, SIAM J. Numer. Anal. 40, (2002), 2195-2218.
[35] R. J. LeVeque and Z. Li, The immersed interface method for elliptic equations with discontinuous coefficients and singular sources, SIAM J. Numer. Anal. 31 (1994) pp. 1019–1044.
[36] R. J. LeVeque and Z. Li, Immersed interface method for Stokes flow with elastic boundaries or surface tension, SIAM J. Sci. Comp. 18 (1997) pp. 709–735.
[37] Z. Li, The immersed interface method using a finite element formulation, Applied Numer. Math. 27 (1998) pp. 253–267.
[38] Z. Li, Immersed interface method for moving interface problems, Numer. Algorithms 14 (1997) pp. 269–293.
[39] Z. Li and K. Ito, The immersed interface method: Numerical solutions of PDEs involving interfaces and irregular domains, Front. Appl. Math. 33, SIAM, Phil. 2006.
[40] Z. Li, T. Lin, Y. Lin, and R. C. Rogers, An immersed finite element space and its approximation capability, Numer. Methods. P.D.E. 20 (2004) pp. 338–367.
[41] Z. Li, T. Lin, and X. Wu, New Cartesian grid methods for interface problems using the finite element formulation, Numer. Math. 96 (2003) pp. 61–98.
[42] T. Lin, Y. Lin, and X. Zhang, A method of lines based on immersed finite elements for parabolic moving interface problems, Adv. Appl. Math. Mech. 5 (2013) pp. 548–568.
[43] T. Lin, Y. Lin, and X. Zhang, Partially Penalized Immersed Finite Element Methods For Elliptic Interface Problems, SIAM J. Numer. Anal. V. 53 (2), 2015, pp.1121–1144.
[44] T. Lin, D. Sheen and X. Zhang, A locking-free immersed finite element method for planar elasticity interface problems, J. of Comp. Phys, 247 (2013) pp. 228–247.
[45] D. Kyeong and D. Y. Kwak, An immersed finite element method for the elasticity problems with displacement jump, Advances in Applied Mathematics and Mechanics, V. 9, No. 2, (2017) pp. 407–428.

[46] I. Ramirere, Ph. Angot, and M. Belliard, A fictitious domain approach with spread interface for elliptic problems with general boundary conditions, Comp. Meth. in Appl. Mech. and Engrng. 196 (2007) pp. 766–781.
[47] Beatrice Riviere, Analysis of a Discontinuous Finite Element Method for the Coupled Stokes and Darcy Problems, J. of Sci. Computing, Vols 22 (2005) pp. 479– 500.
[48] T. Suna, S. Tsudab, K.-P. Zaunerb, and H. Morgana, On-chip electrical impedance tomography for imaging biological cells, Biosensors and Bioelectronics 25 (2010) pp. 1109–1115.

Korea Advanced Institute of Science and Technology, Daejeon, Korea 34141.
E-mail: email:kdy@kaist.ac.kr

Korea Advanced Institute of Science and Technology, Daejeon, Korea 34141.
E-mail: email:woo528@kaist.ac.kr

National Institute for Mathematical Sciences, Daejeon, Korea 34047.
E-mail: email:hyon@nims.re.kr